11

Biocompatible Ceramic – Glass Composite – Manufacturing and Selected Physical – Mechanical Properties

Barbara Staniewicz–Brudnik[1] and Małgorzata Lekka[2]
[1]*The Institute of Advanced Manufacturing Technology, Krakow,*
[2]*The Institute of Nuclear Physics PAS, Krakow,*
Poland

1. Introduction

Biomaterials present specific group of materials, about different composition, structure and properties, which, are accepted by human organism, but some of them (like hydroxyapatite ceramics, bioglass, bioglass – ceramics, modified carbon materials) make connections with alive tissue or take part in its regeneration (Hench L.L. 1998, Krajewski A., Ravaglioli A. 2002).

From historical point of view application of synthetic material for repair of human body are dated from thousand years. It has been discovered, that some Egyptian mummies had dentist denture executed from gold. The first reports about application of ivory as an implementation materials was found in a Greek mythology (Błażewicz S., Stoch L. 2003).

It needs to be mentioned that clinical attempts of refilling of wastes of tissues and bones using a different type of material was initiated before centuries. However, real medical treatment with implementation product manufactured in commercial scale was started in the twentieth century.

In 1902 gold capsules were used for manufactured prostheses of head of femur. From this moment systematical researches on the insertion materials were done. For this group we can classify cobalt – chromium – nickel alloys (Vitallium) that are used in the orthopedics till now (as plates, nails, screws for special applications, dentist implants). Production of polymer materials opened new possibilities.

From 1930 polymetacrylan methylu (PMMA) has been used in the dentistry as a cement fulfills and in the jointing process of metallic bones prostheses, particularly in the case of hip and knee joints.

Application of corundum material by Boutin in the 1972, for manufacturing the elements of joint prostheses was the crucial moment. The following properties have revolutionized the quality of the prostheses: high strength, low friction coefficient, low degree of wear and good biocompatibility (Jaegermann Z., Ślósarczyk A. 2007)

The corundum bioceramics manufactured in different forms (dense, macro and micro porosity) makes many functions during the repair intervention. However, use of many of these materials has experimental character and they are on the clinical stage, there is also

another big, commercial group of products that are applied in the clinical practice (Biolox, Synatite, Endobone, Neobone, Cerabone) (Jaegermann Z., Ślósarczyk A. 2007, Jaegermann Z., et al ,2006).

The newest trend in the regenerative medicine area is tissue engineering, which aimes to obtain medicines and decrease number of complications.

Biocompatible alumina composites are a new generation of ceramic glass materials used in tissue engineering (Jaegermann Z. 2005, Szarska S., et al, 2008 Staniewicz – Brudnik B. et al, 2010). Biomaterials substrates (inorganic, polymeric, hybrid) are two – or three dimensional scaffold, which inhabits the cells (eg fibroblasts) by growing them in vitro, and then the resulting product material and cell is implanted in place of the defect (Chen Q. Z., et al 2008, Brovarone C., Verne E. 2006). The main task of such a scaffold is the physical support for cells and the control of their proliferation, differentiation and morphogenesis (Sachlos E., Czernuszka J. T. 2003).

The basic criteria that should have the substrates (Teramoto H., et al, 2005, Staniewicz – Brudnik B., Lekka M., Bączek E. 2010, Czechowska J., Ślósarczyk A. 2011) are formulated as follows:

- the substrate should contain open pores that connect to each other about the right size to inclusion of cells, then tissues and their vascularity;
- they should have appropriate chemical properties (bioactivity, non – toxic) to promote attachment of cells to substrates, their differentiation and multiplication, mechanical properties (tensile strength, torsion, hardness, Young's modulus) close to the natural materials;
- they should be made of materials with controlled biodegradability (biosorption), so that tissue could be replaced after a specified time basis ;
- do not cause adverse reactions (including allergic)
- they should be easily manufactured in various shapes and sizes.

Taking into considerations all these above requirements the substrates were synthesized, which are biocompatible corundum glass system composites. Biocomposites by combining the characteristics of these materials (Al_20_3, glass) allow to achieve unique properties such as high mechanical strength, crack resistance, high biocompatibility and bioactivity (Hee – Gon B., et al, 2008, Abo – Mosallam H.A., et al, 2009).

The aim of our work is to obtain corundum- glass biocomposites – meeting the above criteria, obtained in a simple, inexpensive and energy efficient way.

The usefulness verification of new substrates was based on short -term cultures of fibroblast human skin of CCL 110 line from Prochem company and mouse preosteoblasts MC3T3 – E1 Subclone14 from the same company.

2. The effect of mechanochemical treatment of submicrocrystalline sintered corundum grains on their certain physical – Mechanical properties

2.1 Submicrocrystalline sintered corundum grains

Submicrocrystalline sintered corundum grains is a new generation of alfa type aluminum oxide with ultradispersive structure, which was obtained by transformation of sol – gel

process of aluminum oxide by using Mg0, L_2O_3, Nd_2O_3, Y_2O_3 as modificators. Abrasive grains consist of Al_2O_3 plates about 0.5 – 1 μm joint by needle bridge of $MgLaAl_{11}O_{19}$ spinel type. Submicrocrystalline sintered corundum grains have in comparison to conventional corundum materials higher strength (90 MPa, conventional 85 MPa), hardness (20 – 22,5 GPa, conventional 18,5 – 21 GPa) with simultenous increase of fracture toughness. Commercial names of these materials are cubitron, Seeded Gel and Blue Sapphire (Niżankowski Cz. 2002, Markul J. 2008).

The submicrocrystalline sintered corundum grains about 150 granulation (125-150 μm) have microhardness of 21.5 Gpa. They were milled for 10, 15, 20, 25 and 30 hours in the planetary mill Pulverisette 6 type produced by Fritsch Company, in the agate chamber with agate balls in the ethanol addition as a slide agent. The grains samples were removed from the chamber after determined times (10, 15, 20, 25, 30 hours) and taken for the further research procedure. The X – ray research works were conducted on the PW 1710 X – ray diffractometer with cobalt lamp at the range of 2Θ angle from 20^o – 90^o. The phase identification and calculation of percentage contents and structure parameters were done using EVA program by Brucker Company.

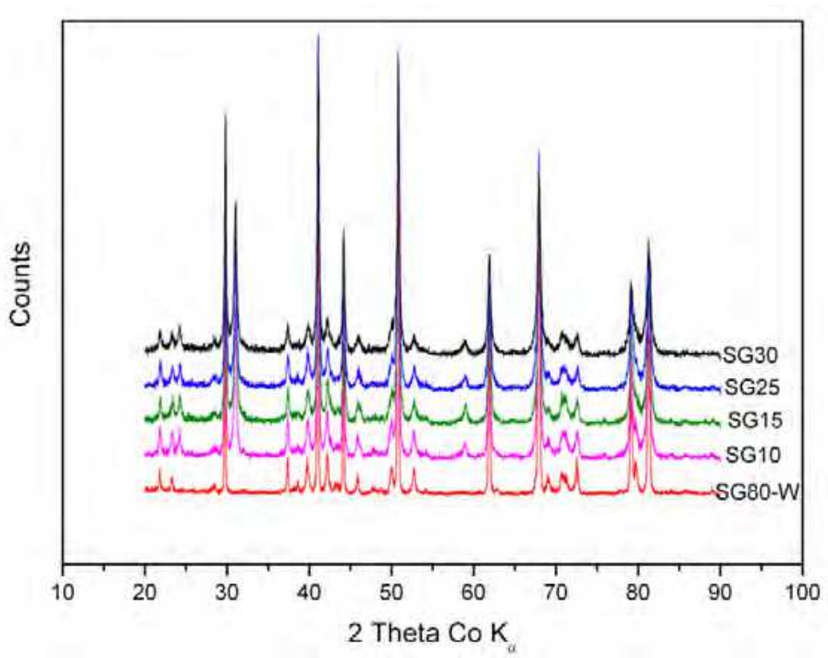

Fig. 1. The X – ray diffraction images of the samples before and after milling for 10, 15, 25, 30 hours.

Basing on this this research in the initial samples of submicrocrystalline sintered corundum the following phases were identified:

α – Al_2O_3 with romboedric structure
kappa – Al_2O_3 with orthoromboedrical structure
δ – Al_2O_3 with orthorombic structure
non – stoichiometric (spinel) compound – $(Mg_{0,03}\ Al_{0,35})\ (Al_{1,68}\ Mg_{0,30})\ O_4$ with cubic structure.

In the milled samples low – temperature quartz (SiO_2) appeared, coming from the used agate balls during the milling process.

The contents of α – Al_2O_3 phase decreased in a benefit of kappa – Al_2O_3, phase, contents of δ – Al_2O_3 was on the same level at different parameters of crystallographic lattice. Lattice parameters of spinel decreased.

Compounds	Time of milling / Structure	Laticce parameters [A°]				
		0	10	15	25	30
Corundum α-Al_2O_3	rombo.	a=4.75970 α=90° b=4.75970 β=90° c=12.9950 γ=120°	a=4.75970 α=90° b=4.75970 β=90° c=12.9950 γ=120°	a=4.75970 α=90° b=4.75970 β=90° c=12.9950 γ=120°	a=4.75970 α=90° b=4.75970 β=90° c=12.9950 γ=120°	a=4.75970 α=90° b=4.75970 β=90° c=12.9950 γ=120°
κ-Al_2O_3	ortorombic	a=4.83400 α=90° b=8.30960 β=90° c=8.93530 γ=90°	a=4.83400 α=90° b=8.30960 β=90° c=8.93530 γ=90°	a=4.83400 α=90° b=8.30960 β=90° c=8.93530 γ=90°	a=4.83400 α=90° b=8.30960 β=90° c=8.93530 γ=90°	a=4.83400 α=90° b=8.30960 β=90° c=8.93530 γ=90°
Magnesium alumi - nium oxide ($Mg_{0.63}Al_{0.35}$)($Al_{1.68}Mg_{034}$)O_4	cubic	a=8.25958	a=8.24575	a=8.17760	a=8.17760	a=8.17760
Aluminium oxide δ–$A\lambda_2O_3$	ortorombic	a=8.02684 α=90° b=7.98915 β=90° c=11.63293 γ=90°	a=7.90755 α=90° b=7.95600 β=90° c=11.67196 γ=90°	a=7.99681 α=90° b=7.95600 β=90° c=11.779313 γ=90°	a=7.97367 α=90° b=7.98252 β=90° c=11.82810 γ=90°	a=7.99350 α=90° b=7.95600 β=90° c=11.71100 γ=90°
Low temperature quartz - SiO_2	hexagonal	-	a=4.92000 b=4.92000 c=5.42000	a=4.92000 b=4.92000 c=5.42000	a=4.92000 b=4.92000 c=5.42000	a=4.92000 b=4.92000 c=5.42000

Table 1. Lattice parameters of individual phases of submicrocrystalline sintered corundum determined from X – ray measurement.

The grains composition measurement were done using Sedigraph 5100 X – ray analyzer (Micrometrics Company). Suspensions from research samples were prepared using solution of distillated water and 0,5% sodium pyrophosphate as a sediment liquid. Grain composition was determined in the range of 100 to 0,2 μm. The measurement results are shown as the cumulative and populative curves in Fig. 2 and 3 respectively.

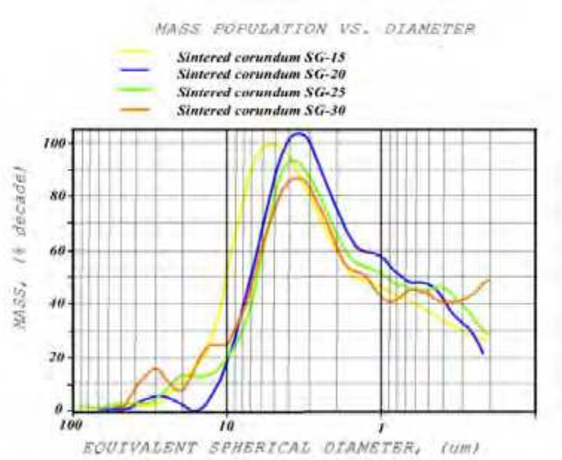

Fig. 2. Populative curves of submicrocrystalline sintered corundum grains after milling for 15,20,25,30 hours.

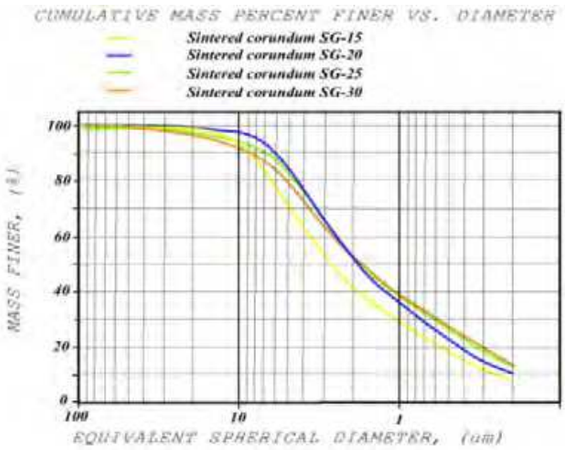

Fig. 3. Cumulative curves of submicrocrystalline sintered corundum grains after milling for 15, 20, 25, 30 hours.

SG – 10 hours – 20 – 1 μm
SG – 15 hours – 10 – 1 μm
SG – 20 hours – 8 – 1 μm
SG – 25 hours – 6 – 1 μm
SG – 30 hours – 6 – 1 μm.

The second population of grains was distinguished on the diagrams that had about 1 μm size with following percentage contents:

SG – 10 hours – 23,6 %
SG – 15 hours – 29,0 %
SG – 20 hours – 35,7 %
SG – 25 hours – 38,9 %
SG – 30 hours – 38,9 %.

The above data indicate that the thickest grains are complementary milled and consequently the contents of ultrafine particles increases. For samples milled for 25 and 30 hours no significant differences in the grains compositions were observed in the entire measuring range. This can be explained by the formation of grains agglomerates, difficult to break even using ultrasonic method.

The specific surface area of samples was determined by S_{BET} physical adsorption of nitrogen at temperatures of liquid nitrogen from the equation Braunaura – Emmett – Teller. For calculations based on the data from the adsorption isotherms the relative pressure at the range p/p_0 0.06 – 0.10 were used. Measurements of specific surface area S_{BET} expressed in m^2/g showed the prolonged milling of samples of submicrocrystalline sintered corundum caused a systematic increase in the specific surface area (from 0.1 m^2/g for the initial sample to 16.4 m^2/g for the sample milled for 30 hours). The greatest effect was achieved after 10 hours milling in relation to the initial sample and after 30 hours of milling in relation to the sample milled for 25 hours and values were 6.4 m^2/g and 3.4 m^2/g respectively.

Sample/fraction below	SG-10	SG-15	SG-20	SG-25	SG-30
40 µm	99.4	100.0	100.0	100.0	100.0
20 µm	95.8	99.3	99.0	97.6	97.2
10 µm	81.7	93.0	97.9	94.0	91.6
5 µm	59.6	71.2	85.0	83.0	79.5
2 µm	34.7	42.3	52.3	53.7	52.1
1 µm	23.6	29.0	35.7	38.9	38.6
0.5 µm	14.8	18.3	22.6	26.9	27.7
0.2 µm	6.1	7.6	10.3	13.1	13.5
Mediane, µm	**3.70**	**2.68**	**1.85**	**1.72**	**1.72**

Table 2. Granulometric analysis of grains (percentage of the fraction below).

Microscopic observations were performed on scanning electron microscope JSM 6460 LV JEOL Company in the range of low and high vacuum, at 20 kV accelerating voltage. SEM and COMPO images were observed at 100x, 400x, 1000x and 2500x magnifications. In these images elongated, irregular grains with sharp edges were present. In the samples milled 10, 15, 20 hours a few large grains and the increased amount of fine grains was observed. In the sample milled for 30 hours cluster of agglomerates appeared.

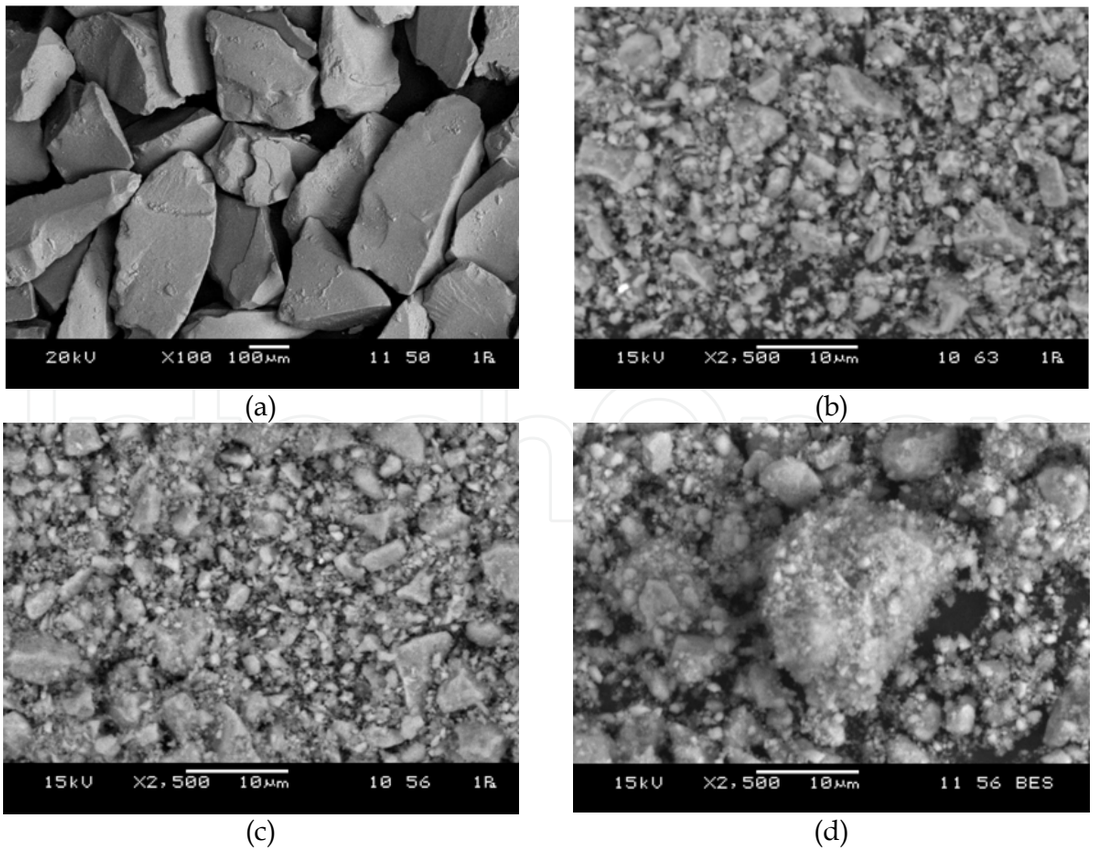

(a) (b)

(c) (d)

Fig. 4. SEM image of submicrocrystalline sintered corundum grains:

a. before milling (100x magn.)
b. after 15 hours of milling (2500x magn.)
c. after 20 hours of milling (2500x magn.)
d. after 30 hours of milling (2500x magn.)

2.2 Glass of $Ca0 – Si0_2 – P_20_5 – Na_20$ system

Glass calcium – silicate – phosphate from the system $Ca0 – Si0_2 – P_20_5 – Na_20$ was obtained at 1350^0C by fritting method. Initial materials were:

Calcium carbonate – analytically pure
Sodium phosphate – analytically pure
Silicon dioxide – pure
sodium carbonate – analytically pure.

Three frits were obtained from completely transparent with bluish aquamarine to milky opaque amber colour. Frits were milled in the planetary mill Pulverisette 6 type (Fritsch Company), in the agate chamber with agate balls by 5, 10, 15 and 20 hours with the addition of distilled water. Samples were removed after a certain time subjecting them to further test procedure. A similar procedure was used as in the case of submicrocrystalline sintered corundum grains.

The resulting glass was subjected to chemical analysis on the spectrometer ARL Advant'XP by X – ray fluorescence spectral method. The results of oxide glass compositions were very closed to the calculated theoretically composition, taking into account 10% of the volatility of phosphorus.

Observations of the glassy frits using the scanning electron microscope revealed the presence of elongated grains, irregularly shaped with sharply outlined edges. After prolonged milling a few large grains and clusters of small grains were visible.

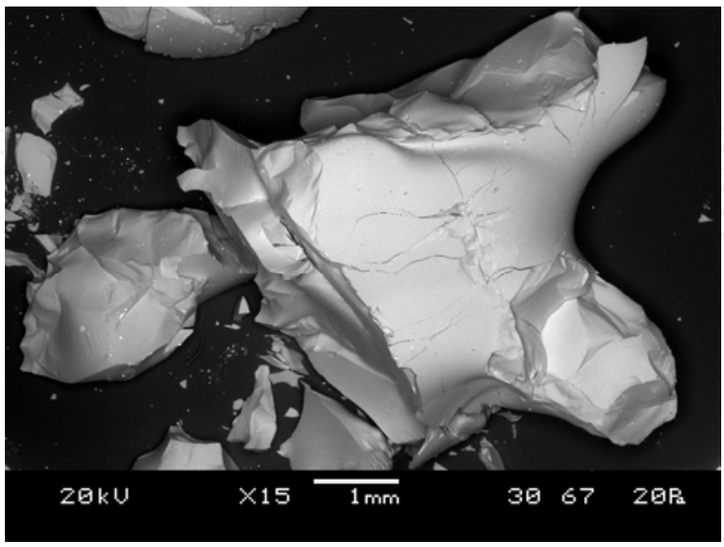

Fig. 5. Glass FB3 system after fritting process.

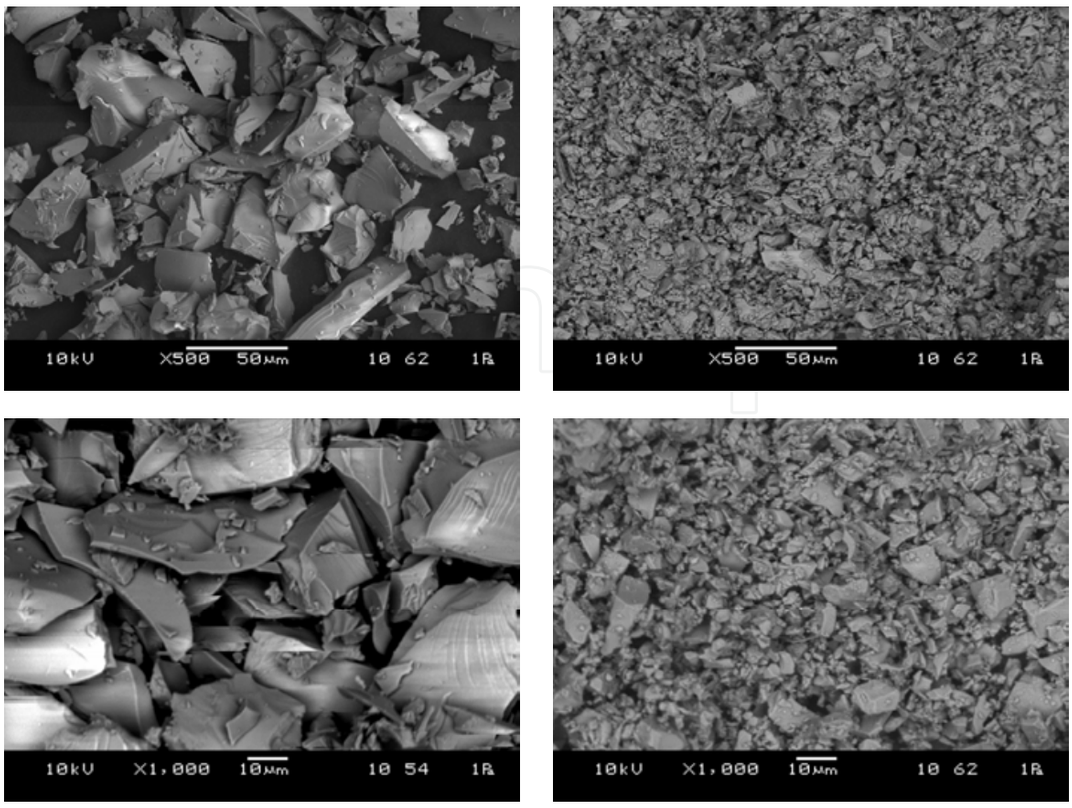

Fig. 6. SEM images of glass FB3 system milled for 5 and 20 hours.

Prolonged milling did not significantly influence the growth of specific surface area of glass system. Only after 20 hours of milling glass system specific surface area was doubled. The reasons for this phenomena might be explained by the acting of large cohesive forces of glass particles.

The densities of glasses were determined by helium method using the pycnometer AccuPyc 330. Analysis of results showed that these glasses belong to a light group of glass (density of 2.65 – 2.70 g/cm^3). Knowing the density and specific surface area and using the formula:

$$2r = \frac{6}{S_{BET} \cdot d} \tag{1}$$

diameters of the grains were calculated. Only after 20 hours of milling the grain sizes were nearly two times decreased from 2.47 µm to 1.17 µm diameter.

Time milling	Value of specific surface area m^2/g	Average size of grains µm
5 hours	0,9159	2,47
10 hours	0,9553	2,36
15 hours	1,1964	1,89
20 hours	1,9241	1,17

Table 3. Average grains sizes of glass FB3 system after milling by 5, 10, 15, 20 hours and related them specific surface areas.

DTA and DTG studies allowed us to determine the glass temperature of vitrification (FB1 – 538 ^{0}C, FB2 – 535 ^{0}C, FB3 – 525 ^{0}C) and temperature of dilatometric softening point (FB1 697 ^{o}C, FB2 700,9 ^{o}C, FB3 711,9 ^{0}C). DTG curve for the glass FB3 system indicated a normal weight loss about 1 wt.% for temperature of 600 ^{0}C. In case of glass FB2 system the mass loss, about 5wt% was far too large. This suggested the presence of internal defects, consisting in incorporating the occluded water and CO_2 particle in the glass structure. This was confirmed by the investigation using the DTA apparatus containing the gas analyzer, indicating volatilization of particles at a temperature of 150 °C, for H_20 and at a temperature of 400 ^{o}C for CO_2 particles.

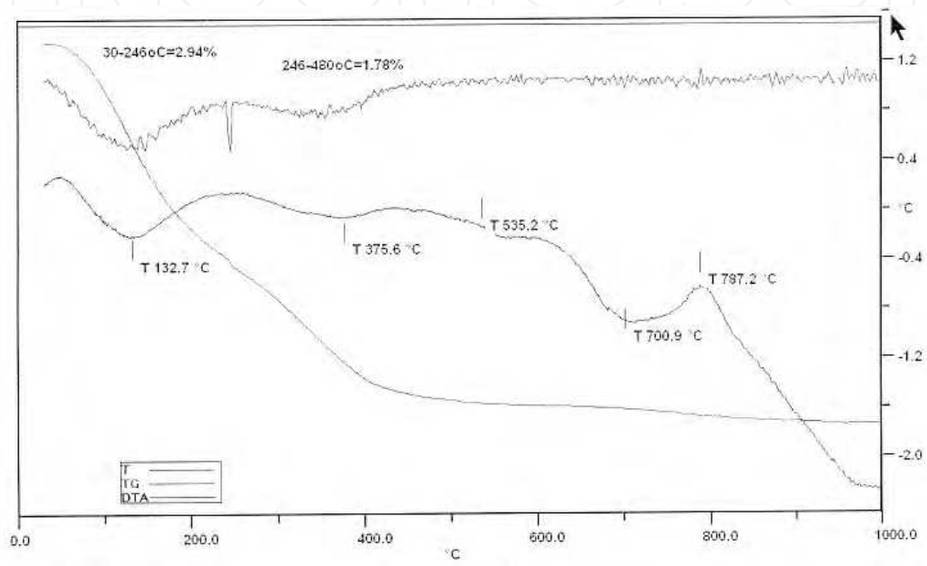

Fig. 7. DTA and DTG of glass FB2 system.

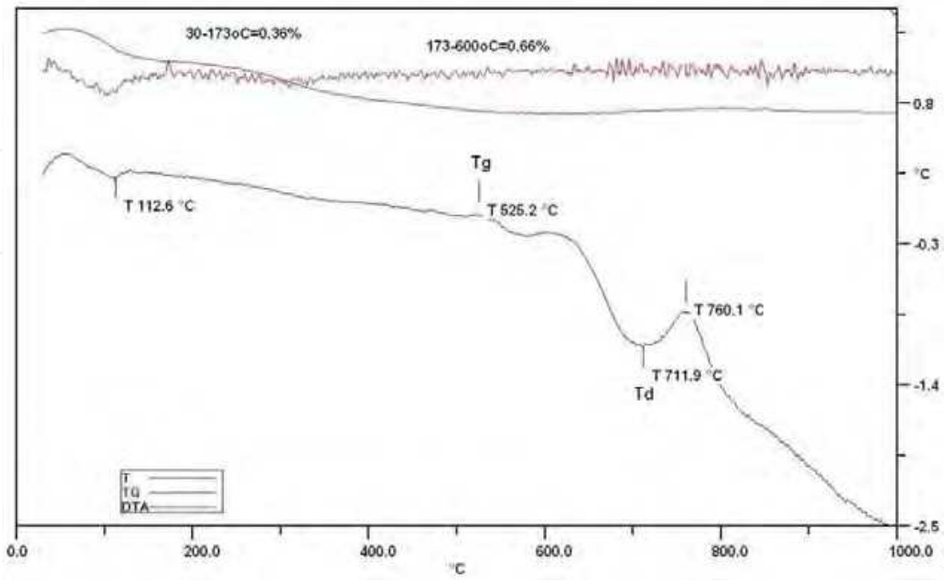

Fig. 8. DTA and DTG of glass FB3 system.

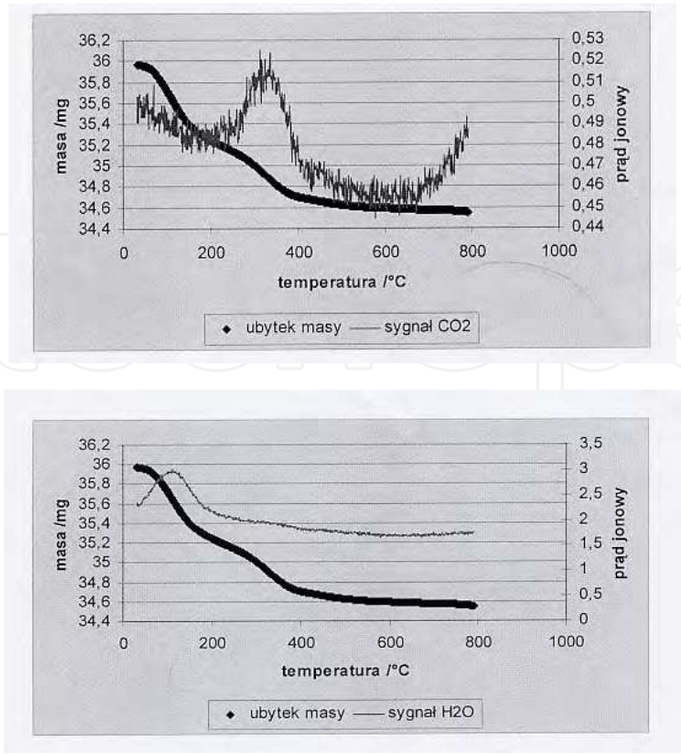

Fig. 9. DTG of glass FB2 system with gas analysis.

Microhardness measurements were carried out using the micro tester FM7 with 100g load. The results show that these are hard glass systems within 5.5 – 6.0 GPa hardness.

Wettability research test of glass system to plate substrates from submicrocrystalline sintered corundum carried out at high temperature microscope MH02 by sessile – drop method showed that the glass FB3 was not gasified, there was no significant change in the dimensions of the swelling and contact angle theta was about 45^0.

a) 110°C a) 904°C a) 1010°C

Fig. 10. Wettability of glass FB3 system on the substrate from submicrocrystalline sintered corundum, a) 110°C, b) 904°C, c) 1010°C.

For further research the submicrocrystalline sintered corundum milled for 20 hours and the glass FB3 system were chosen because of the obtained value of specific surface area of corundum and the properties stability of glass.

3. Biocomposites

The composites containing a matrix from submicrocrystalline sintered corundum and bioglass of $Ca0 – Si0_2 – P_20_5 – Na_20$ system (FB3) in 10, 20 and 30 wt.%, obtained by powder metallurgy technique, in the process of free sintering in air atmosphere, in the electric furnace. Bioglass of the $Ca0 – Si0_2 – P_20_5 – Na_20$ system was obtained by fritting process at 1350 ^oC using an electric furnace.

The composites were obtained with two techniques:

- cold pressing and sintering
- cold pressing, isostatic densification and sintering.

Samples of small (Ø10x2) and large (Ø16x5) size were pressed on the screw press, and after they were isostatically densified or not. The heat treatment was performed without the mould in an electric furnace in air, according to the established characteristics of isothermal soak, at maximum temperature at the time of 2 hours.

Phase composition of biocomposite samples was identified using X – ray diffractometer August Siemens Type D 500 Cristal Reflex with copper lamp with monochromatic radiation.

The phases composition were determined for the samples doped with 10 wt.% bioglass admixture isostatic densification or without densification (w1ssc), the identity of the spectra was found in both cases, suggesting the identity of the phase composition of the samples, regardless of the method of obtaining. In samples following phases were identified : alpha and kappa – Al_20_3 (kappa in the trace amounts), anortit – aluminum calcium silicate – $CaAl_2(Si0_4)_2$, sodium aluminum silicate $NaAlSi0_4$ and quartz $Si0_2$.

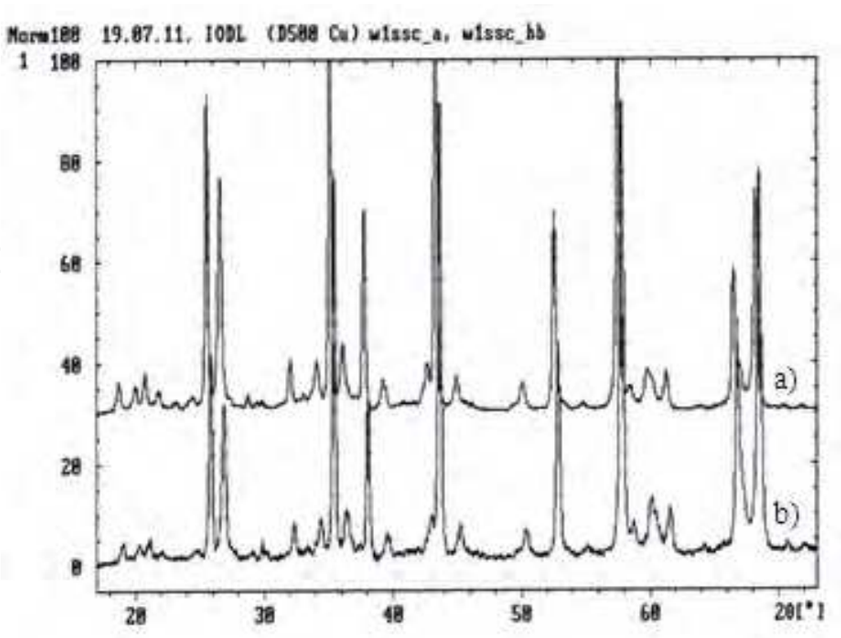

Fig. 11. The XRD spectra for w1ssc samples a) with isostatic densification, b) without densification.

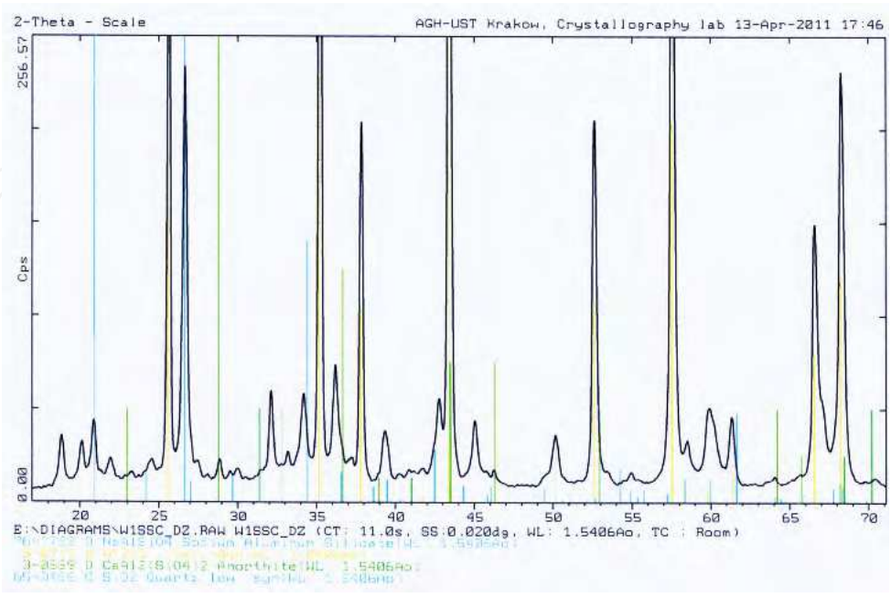

Fig. 12. Identification of XRD spectra for w1ssc isostatically densified sample.

Additionally were made the samples with 20, 30 wt.% glass admixture without isostatic densification. It was found, that the phase composition did not change very much.

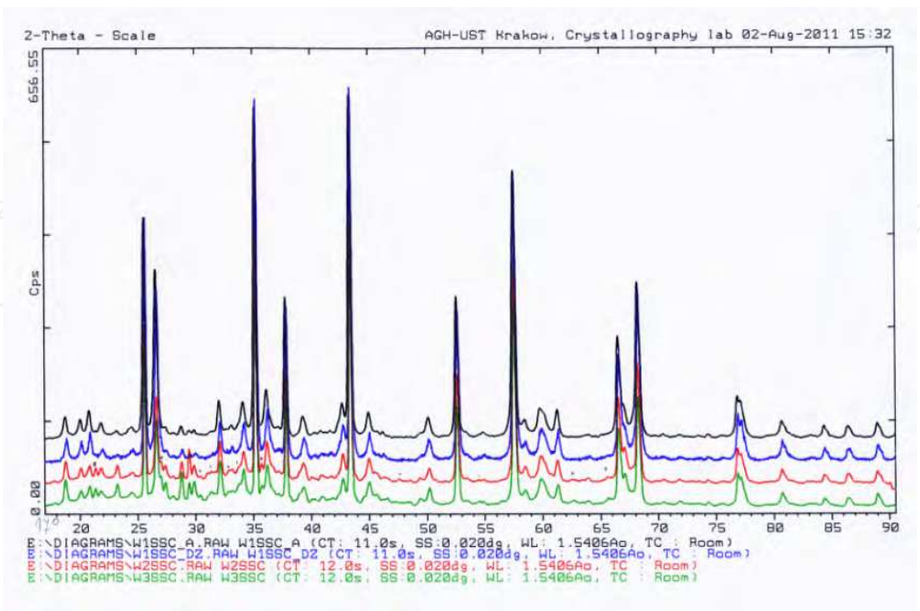

Fig. 13. The XRD spectra for w1ssc, w2ssc, w3ssc samples without densification.

Phase	Strukture	Crystalographic parameters
SiO_2	hexagonal	a = 4,913 c = 5,405
$MgAl_{11}LaO_{19}$	hexagonal	a = 5,582 c = 21,942
CaO	Face – centered cubic	a = 4,797
$NaAlSiO_4$	cubic	a = 7,37
P_2O_5	Face centered orthorhombic	a = 16,3 b = 8,14 c = 5,26 a/b = 2,00246 c/b = 0,64619
Al_2O_3	rhombohedral	a = 4,758 c = 12,991
$CaAl_2(SiO_4)_2$	triclinic	a = 8,21 b = 12,95 c = 14,16 a/b = 0,63398 c/b = 1,09344

Table 4. Crystalographic identification of phase composition.

Microscopic observations with the electron microscopes Jeol JSM 6460 LV type were performed in high vacuum (~ 1,3 x10^{-3}Pa) at 20 kV accelerating voltage, magnification 20x, 100x and 1000x using of BEC image. Microscopic observations carried out with the scanning electron microscope revealed the differences in the microstructure of samples after isostatic densification or without densification. Microstructures of composites contained grains of irregular shape and varying dimensions and pores. The dimensions of grains were in the range below 1 μm to several μm. Leeks (pores) had a varied shape and dimensions of the order of several micrometers. Samples obtained without densification were more porous; but having more smaller pores (mesopores). Isostatically densified samples had dense microstructure with a small amount of larger pores. Photos of samples formed by various techniques are presented in Fig. 14, 15 under magnification 1000x.

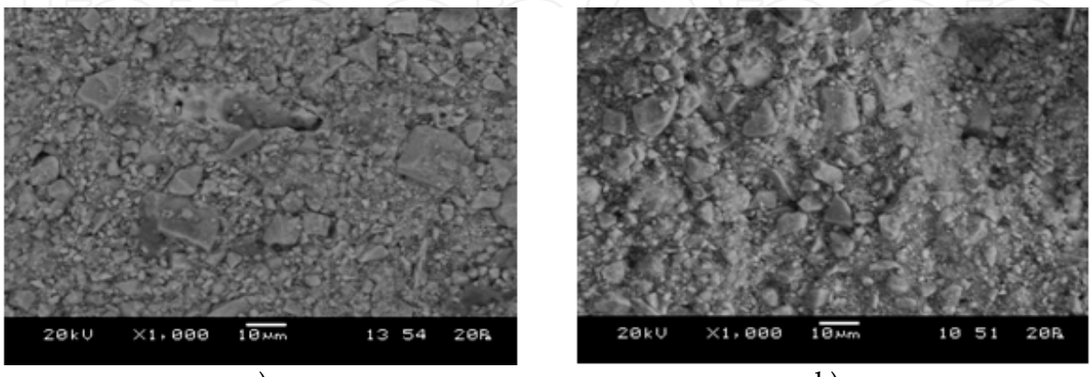

a) b)

Fig. 14. The SEM observations of the sample W1ssc, magn. 1000x; a) with isostatic densification, b) without densification.

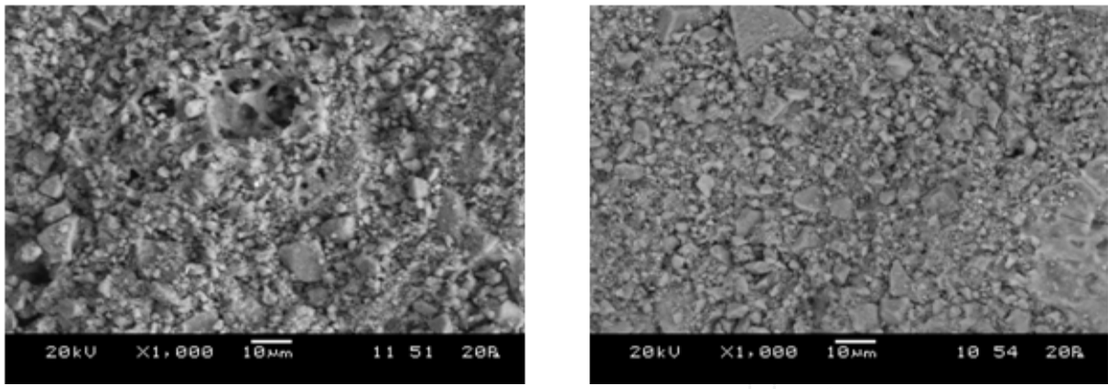

a) b)

Fig. 15. The SEM observations of the sample W2ssc, magn. 1000x; a) with isostatic densification, b) without densification.

Measurements of the real density (d_{real}) – of powder samples and helium density (on tablets Ø 16x5mm) were performed using helium pycnometer AccuPyc1330 Micrometrics company. Before the relevant measurements of the samples were initially desorbed by a 10 – fold pure helium flushing. Five parallel measurements were done for each sample. The results were used to calculate the closed porosity. Measurements of apparent density (d_{ap}) and total porosity (Pc) were carried out using GeoPyc density analyzer, model 1360 manufactured by Micrometrics. Ten simultaneous measurements were made for each sample. Apparent density (g/cm^3), the volume of pores in the material Vc (cm^3/g) and total porosity (%) were determined.

Sample/ parameter	W1 without dens.	W1 isostat. dens.	W2 without dens.	W2 isostat. dens	W3 without dens.	W3 isostat. dens
d_{real}, g/cm^3	3,6150 ±0,0050	3,6150 ±0,0050	3,5296 ±0,0193	3,5296 ±0,0193	3,4743 ±0,0252	3,4743 ±0,0252
d_{hel}, g/cm^3	3,6684 ±0,0089	3,5457 ±0,0109	3,5010 ±0,0167	3,5237 ±0,0030	3,3942 ±0,0249	3,4319 ±0,0402
$d_{apperend}$, g/cm^3	2,2821 ±0,0054	2,3179 ±0,0052	2,1564 ±0,0070	2,2516 ±0,0097	1,9637 ±0,0044	2,0442 ±0,0052
V_{pores}, cm^3/g	0,166	0,149	0,178	0,160	0,215	0,198
V_{macro}, cm^3/g	0,161	0,146	0,176	0,159	0,214	0,197
V_{mezo},cm^3/g	0,005	0,003	0,002	0,001	0,001	0,001
P, %	36,9	35,9	38,9	36,2	43,5	41,2
S_{BET}, m^2/g	1,99	1,45	1,02	0,88	0,89	0,50

Table 5. Density and porosity of biocomposite samples.

Studies of real density of the sample d_{real} (Table 5) showed that, regardless of the method of preparation, with increasing glass content in the composite the real density decreases (from 3,615 to 3,474 g/cm^3). It resulted from the different density of submicrocrystalline sintered corundum (3,887g/cm^3) and glass FB3 system (2,564 g/cm^3).

The results of determining the apparent density and the skeleton of both open and closed pores became evident that the apparent density decreases with increasing glass content, in both cases of isostatic densification or without densification, but the value of the apparent density of isostatically densified samples was higher than of samples without densification, what resulted from the process of obtaining . Based on density measurements of helium and the actual porosity of the closed set Pz results showed that in the test samples there were present opened pores and closed pores were in negligible volume. Specific surface samples with increasing S_{BET} bioglass content decreased in both cases (samples isostatically densified or without densification). The values of SBET in the 0,5 to approximately 2,0 m^2/g were testified by low content of mesopores which volume ranged from 0,001 to 0,005 cm^3/g.

Visible is that the total porosity increased with increasing bioglass content for both isostatically densified samples (from 0,146 to 0,197cm^3/g) and without densification (from 0,161 to 0,214 cm^3/g) containing mainly macropores with dimensions greater than 0.1 microns, which resulted from an increased quantities of bioglass mainly having opened pores.

Measurements of surface area (S_{BET}) were performed using the multifunctional apparatus (ASAP 2010, Micromeritics American company) for measuring surface area and porosity. The specific surface area was determined by physical S_{BET} nitrogen adsorption at liquid nitrogen temperature (77K) from the equation Brunauer – Emmet – Teller (the theory of multilayer adsorption). Before the measurement surfaces of the test samples were subjected to desorption at temperature 1050^{o}C, in vacuum and flushing with pure helium. Sample degassing time was about 8 hours. Surface degassing state was controlled in automatic mode.

The specific surface area calculations based on data from the adsorption isotherms of the relative pressure range p/p_0 from about 0,06 to about 0,20% and the volume and dimensions of the mesopores were calculated using p/p_0 of 0,97%.

Geometric structures of the biocomposites samples surface were determined using the TOPO 01vP profilometer, by measuring the surface topography parameters (Ra, Rz, Rt), the image of 2D and 3D ,profile material rate and amplitude distributions of the ordinates.

The geometric structure of the surface isostatically densified or without densification samples (w1ssc) have been evaluated by measuring surface topography performed using TOPO 01vP profilometer developed and produced in IZTW. There were defined the basic parameters of roughness (Ra, Rz, Rt). In the isostatically densified sample porosity effect on profile was visible (few large cavities- inequality) .This was confirmed by image analysis of 2D and 3D. Participation of the linear bearing and amplitude distribution of the ordinate was shifted toward negative values.

The profile roughness of sample without densification has more blurred shape, with more small pits and a few large inequalities compared with the profile of the isostatic densification sample. It was testified by the image analysis of 2D and 3D. The amplitude distribution of the ordinate showed the presence of inequality – type cavities.

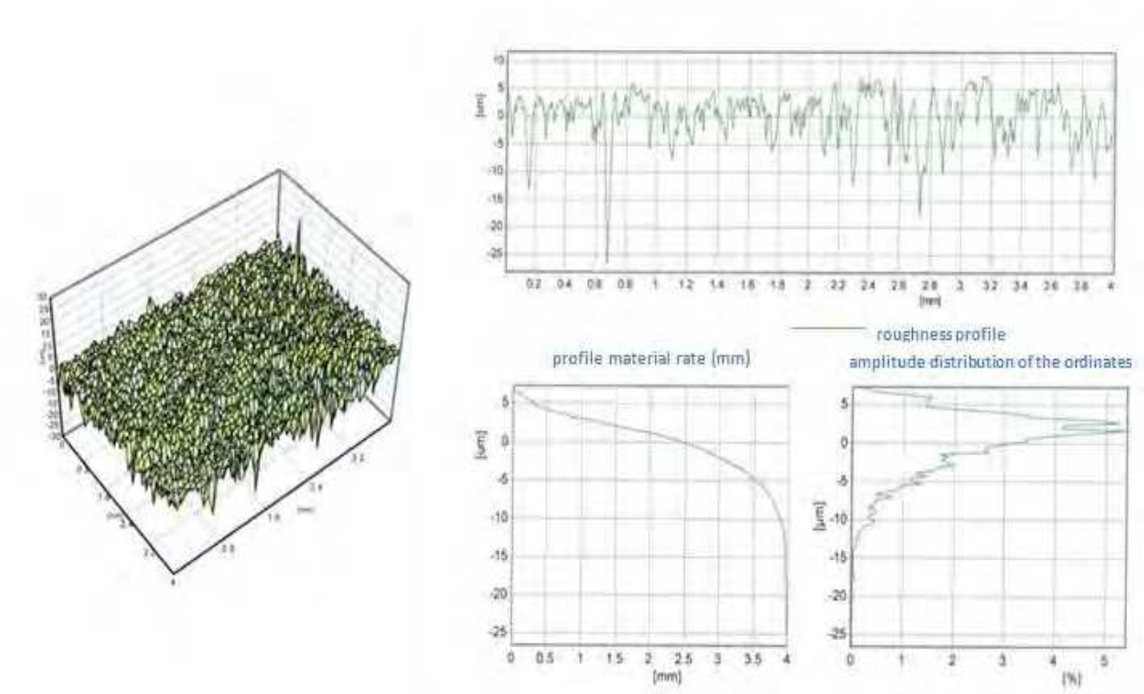

Fig. 16. The image of 2D and 3D, along with a profile material rate and amplitude distribution of the ordinates for isostic densification w1ssc sample.

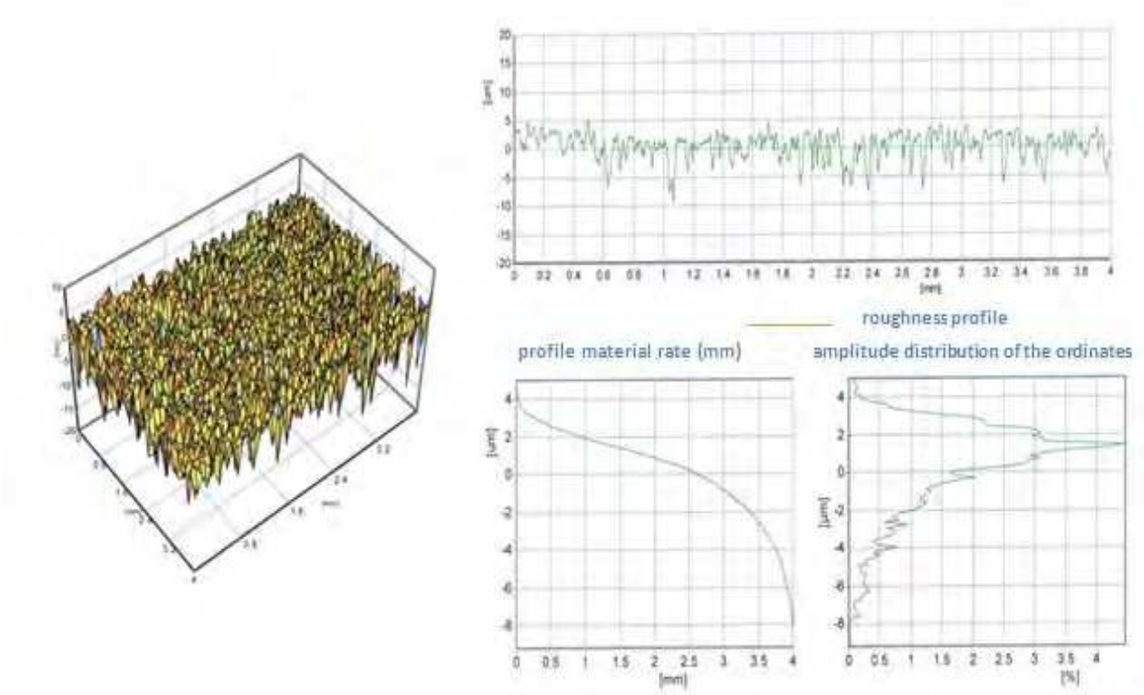

Fig. 17. The image of 2D and 3D, along with a profile material rate and amplitude distribution of the ordinates without densification w1ssc sample.

4. Short term culture of the fibroblast human skin CCL 110 line and mouse preosteoblasts MC3T3 – E1 Subclone 14 on these substrates

The usefulness verification of these research substrates (w1ssc, w2ssc, w3ssc) for cell culture were checked for short – term culture of human skin CCL line and mouse preosteoblasts MC3T3 – E1 Subclone 14 CRL 2594 line.

4.1 Materials and methodology

Bioglass sterilization. The surfaces used for cell growing were w1ssc, w2ssc, and w3ssc. Before seeding the cells, the following protocol for sterilization has been applied. The samples of the bioglass composite (10 mm in diameter and 2 mm in thickness) were immersed in the 70 % alcohol solution for 12 hours. Afterwards, each side of the sample was exposed for 2 hours to UVC light (wavelength of 245 nm), which was provided by a germicidal lamp from a laminar flow chamber (Nuaire Nu 425), at average intensity of 0.1 mW/cm^2 at the working plane. Such sterilized bioglass samples were used immediately for cell growth.

Cell lines. Two types of cell lines were studied:

- human skin fibroblasts (CCL-110, LG Promochem) were cultured in DMEM (Dulbecco's Modified Eagle Medium, Sigma) containing 5 % of fetal bovine serum and 1 % mixture solution of antibiotics (streptomycin, neomycin and penicillin). They were grown at 37^{o}C in an incubator (NUAIRE, USA) providing 95% air / 5% CO_2 atmosphere. Initially, cells were grown in a culture flask (Saarstedt) and when they formed semi-confluent monolayer, they were trypsinized using 0.25% trypsin/EDTA solution (Sigma) and placed into bioglass surfaces for 96 h and 360 h.
- mouse preosteoblasts MC3T3 – E1 Subclone 14 (CRL-2594, LG Promochem). Cells were cultured in Alpha Minimum Essential Medium with ribonucleisides, supplemented with 10% fetal bovine serum (LG Promochem). They were grown at 37^{o}C in an incubator (NUAIRE, USA) providing 95% air/ 5% CO_2 atmosphere. Analogously to fibroblasts, cells were grown in a culture flask (Saarstedt) and when they formed semi-confluent monolayer, they were trypsinized using 0.25% trypsin/EDTA solution (Sigma) and placed into bioglass surfaces for 96 h and 360 h.

Phalloidin staining. To visualize the organization of actin filaments, cells were stained and imaged using fluorescent microscope (the same protocol was applied independently of the cell type). First, cells grown on bioglass surfaces, were fixed with 3.7% paraformaldehyde dissolved in the PBS buffer for 10 minutes, followed by rinsing them twice in the PBS buffer (Phosphate Bufered Saline, Sigma), permeabilization with 0.1% Triton X-100 solution in the PBS buffer. Then, they were again rinsed in the PBS buffer (3x3 minutes). The actin filaments were stained using the solution containing phalloidin labeled with Alexa Fluor 488 (1:200, in PBS buffer, Molecular Probes) for 30 minutes incubation at room temperature. Next the excess of dye was removed by rinsing bioglass surfaces in the PBS buffer. The wet surfaces with stained cells were placed on the microscope slide and immediately imaged.

Fluorescence microscopy. Fluorescence is the ability of organic or inorganic specimen to absorb and subsequent emit of light. The basic function of a fluorescence microscopy is to irradiate the sample with a desired and specific band of wavelengths, and then to separate the much weaker emitted fluorescence from the excitation light. In a properly configured microscope, only the emission light should reach the eye or detector so that the resulting fluorescent

structures are superimposed with high contrast against a very dark (or black) background. The limits of detection are generally governed by the darkness of the background, and the excitation light is typically several hundred thousand to a million times brighter than the emitted fluorescence. In the presented studies, the fluorescence microscope was used to visualize the actin filaments, which were stained with phalloidin labeled with Alexa Fluor 488 that absorb blue light ($\lambda = 495$ nm) and emits green fluorescence ($\lambda = 518$ nm). The images were recorded using Olympus 71X microscope equipped with the 100 W mercury lamp, the MWIG2 filter, and digital camera XC 10 (working under Cell^R program).

4.2 Results and discussion

The visualization of the cell shape has been perform through actin filament staining using phalloidin coupled with Alexa – Fluor 488. Although actin filaments are dispersed within entire cell, they are concentrating mainly in cortex layer beneath the plasma membrane, and therefore they can be used for cell-shape visualization (fig. 18). The cell cultures were performed for single cells grown for 96 hours. The images observed for fibroblasts were better due to the higher amount of actin filaments inside as compared to osteoblats. However, independenlty of the cell type, their shape varied from rounded to the well extended (spindle – like) ones.

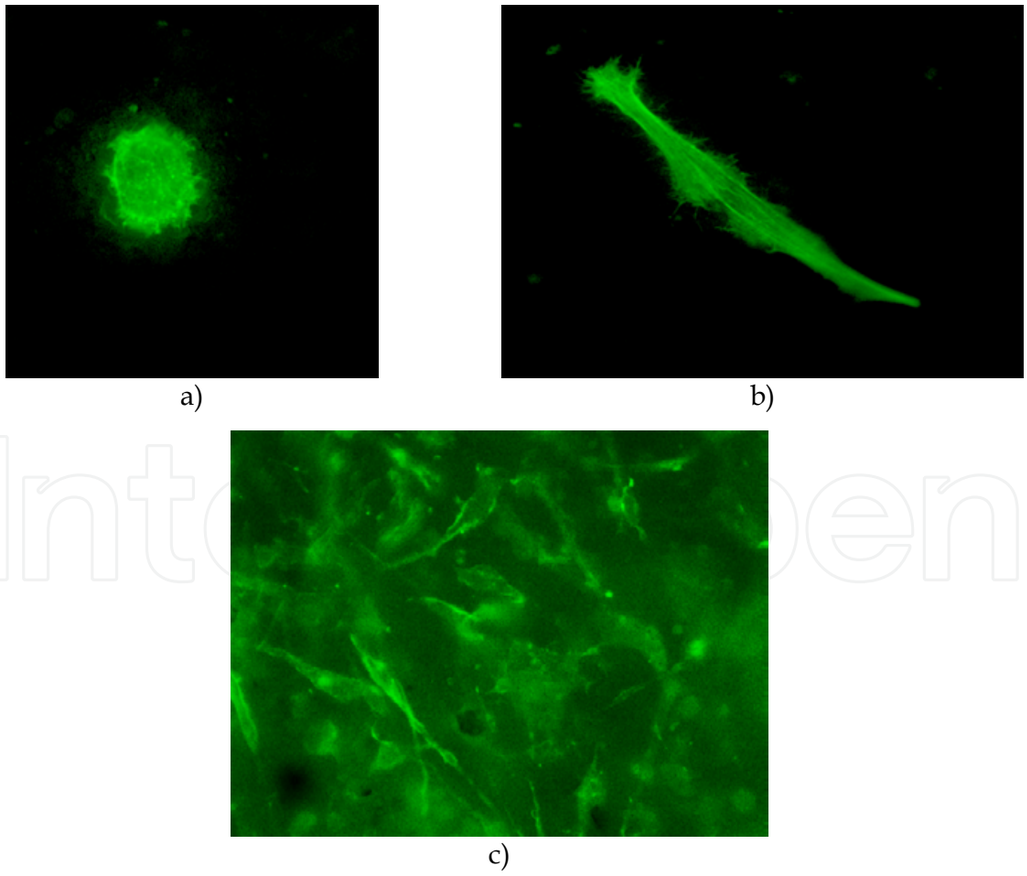

a) b) c)

Fig. 18. Fluorescent images recorded after 96 hours of growth on composites (magnitude 600x), a, b – fibroblasts, c – osteoblasts.

The round cells denotes the cells that starts to detach from the investigated surface. In general, cells spread and grow on rigid substrates if the provided conditions enable them to preserve normal functioning (in such conditions fibroblasts turn into spindle-shaped cells) but they retract, and become round on non-biocompatible ones. The table 6 presents the summary of shapes observed for both fibroblasts and osteoblasts cultured on the studed surfaces W1ssc, W2ssc, and W3ssc.

Composite's surface	Isostatic densification	Cell type	Cell shape
W1ssc	Yes	fibroblasts osteoblasts	spindle-like and round spindle-like
W1ssc	No	fibroblasts osteoblasts	round spindle-like
W2ssc	Yes	fibroblasts osteoblasts	spindle-like and round spindle-like
W2ssc	No	fibroblasts osteoblasts	round round
W3ssc	Yes	fibroblasts osteoblasts	round spindle-like
W3ssc	No	fibroblasts osteoblasts	spindle-like spindle-like and round

Table 6. Summary of cellular shapes cultured on the different composite's surfaces.

To estimate the number of cells present on composite surface, the percentage of cells present on a given sample type was calculated as a ratio of cells present on the studied surface divided by the number of cells cultured on a glass coveslip (2500 and 4800 cells on a glass rounded coveslip with diameter of 10 mm for human skin fibroblats and mouse osteoblasts, respectively).

Figure 19 a and b shows the comparison between the percentage of cells attached to composite surfaces (W1ssc, W2ssc, W3ssc) after 96-hour of growth in culture conditions. In case of fibroblasts, the composite surfaces without densifications manifest larger survival level as compared to those proceed after densification. The isostatic densification results in lower biocompability of the surfaces. The observed drop was from 23% to 11%, 7% to 4%, and 15% to 8% for W1ssc, W2ssc and W3ssc composites, respectively. The worst biocompatible properties were observed for W2ssc sample. The ability of cells to grow on W1ssc and W3ssc was comparable.

Mouse osteoblasts behave similarly. The observed increase was from 18% to 24%, 7% to 11%, and 13% to 19% for W1ssc, W2ssc and W3ssc composites, respectively. Analogously as for fibroblasts, the quality of growing conditions for osteoblasts can be order as follows: the worst biocompatible properties were observed for W2ssc composite, then W3ssc, and W1ssc surfaces are placed.

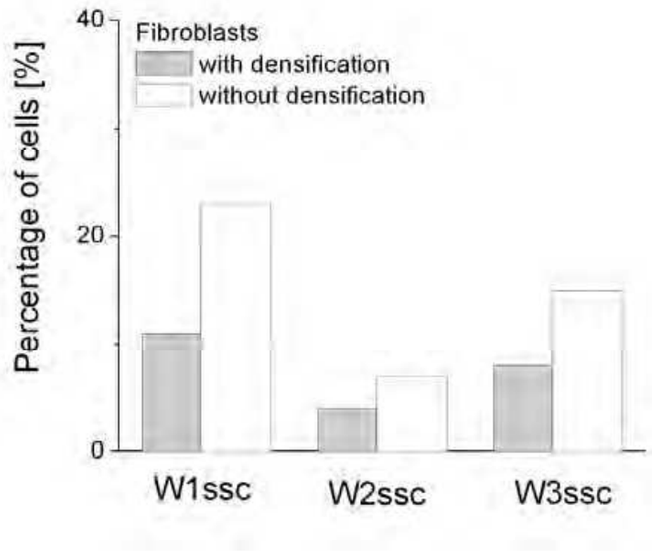

a)

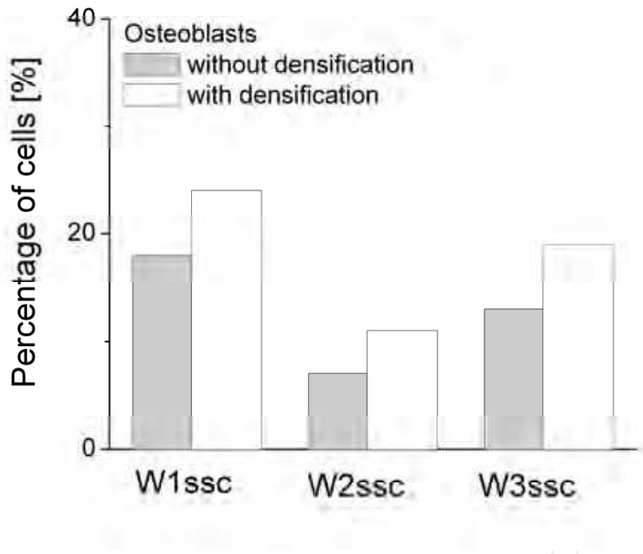

b)

Fig. 19. The percentage of cells (fibroblasts and osteoblasts) present on a surface of composite surfaces.

One of the important conditions that should be provided by biocompatible materials is providing the optimal conditions for cell growth, which can be characterized by the doubling time (Maret D., et. al, 2010, Puttini S., et al, 2009). The chosen cells doubled their amount after 130 and 38 hours for fibroblasts and osteoblasts, respectively, when cultured on Petri dish in optimal conditions. Therefore, this parameter was determined to monitor the changes in their growth. The results are presented in fig. 20 a and b.

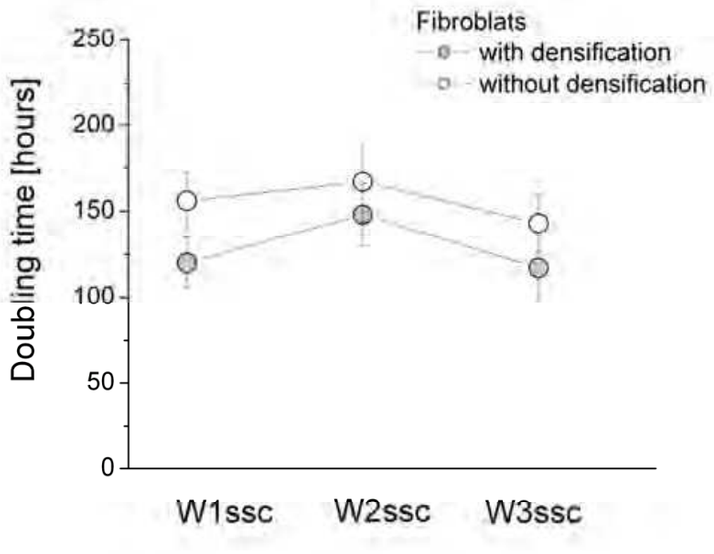

a)

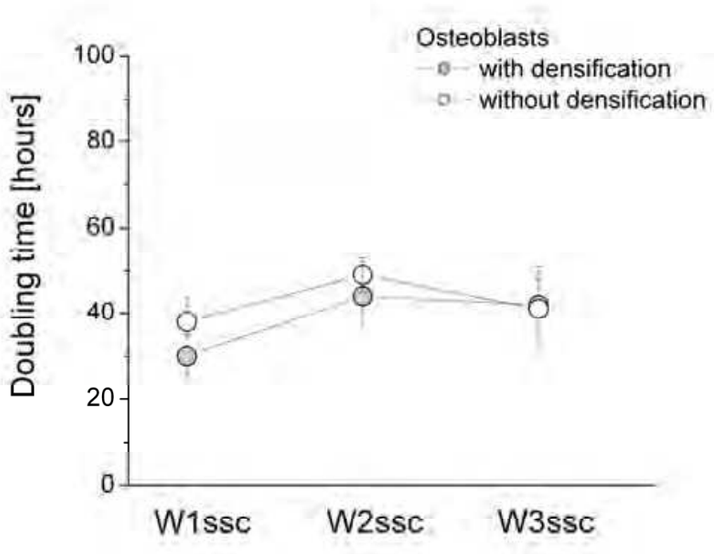

b)

Fig. 20. The percentage of cells (fibroblasts and osteoblasts) present on a surface of composite surfaces.

The doubling time was dependent on the substrate properties. For fibroblasts, the obtained values were 120 ± 15 h, 148 ± 18 h, 117 ± 19 h for composite's surfaces prepared without densification (fig. 20 a). The application of densification step introduces the increase of doubling time to 156 ± 16 h, 167 ± 23 h, and 143 ± 17 h, for W1ssc, W2ssc, and W3ssc, respectively. Longer doubling times correlated well with the lower number of cells present on the corresponding composite's surface. Thus, indicating worse growing conditions for

fibroblasts. Analogously, as for fibroblasts, the doubling time was determined for osteoblasts (fig. 20 b). Also in that case, its value showed a relationship with the number of cells on a composite's surfaces, pointing out the best growing conditions in case of W1ssc surfaces.

5. Conclusions

Based on studies conducted so far can be stated that:

- prolonged milling of submicrocrystalline sintered corundum effectively increased the specific surface area of grains from 0.1 m^2/g for the sample which was not milled to the value 16.4 m^2/g for the sample milled for 30 hours. Particle size distribution after milling for 10, 15, 20, 25 and 30 hours of populative and cumulative curves indicated the multimodal shape with two distinctive ranges of particle size depending on the time of milling. Agglomerated particles were observed after 25 and 30 hours of milling.
- X – ray studies revealed the presence of phases α, kappa, δ and Al_2O_3 and non – stoichiometric composition of magnesium aluminum oxide $(Mg_{0.63}Al_{0.35})$ $(Al_{1.68}Mg_{0.30})O_4$ in initial sample. Additionally, in milling samples the silicon dioxide (quartz) coming from the used agate balls from the planetary mill Pulverisette 6 type appeared.
- in the case of glass of calcium – silicon phosphate system prolonged mechanochemical treatment neither had a significant effect on the increase specific surface area (it was only twice after 20 hours milling from 0.9159 m^2/g in the starting glass system to 1.9241 m^2/g after 20 hours milling), nor on the change of size of glass system grains (from 2.47 μm after 5 hours to 1.17 μm after 20 hours).:
- it was found that the phase composition of w1ssc samples (with or without isostatic densification) was identical regardless of the method of manufacturing. It have been identified for w1, w2, w3ssc samples alfa and kappa aluminum oxide and at w1ssc anorthit $CaAl_2$ $(Si0_4)_2$, at w2ssc, w3ssc $NaAlSi_20_6$ additionally;
- observations of biocomposites substrates for scanning electron microscope showed increased porosity in the samples without densification with large number of small pores. Isostatically densified samples had more compact structure, with a small amount of larger pores;
- the difference between total porosity in the samples after isostatic densification and without densification was evident. The samples without densification have a higher porosity with increasing bioglass system A similar trend is maintained in case of isostatically densified composites; with increasing glass content increases the total porosity, apparent and real density decreases. It may be found that the most common pores in all the substrates is far greater than 0,1 micron;
- the analysis of parameters, diagrams and distributions showed significant asymmetry of the distribution in the negative value direction of unevenness for the both cases. It was bigger for not densified sample.
- the studied composite's surfaces (W1ssc, W2ssc, W3ssc) were characterized by distinct biocompatible properties. The growth of two cell types i.e. fibroblasts and osteoblasts revealed cell – type dependent behaviour.. All substrates without densification seemed to provide better growing conditions for fibroblasts and preosteoblasts while isostatic densification induced worser surface properties for cell growth

6. Acknowledgments

This work was partially supported by the project SMW (Single Molecule Workstation), grant agreement number 213717 (NMP4 - SE - 2008 - 213717).

7. References

Abo – Mosallam H.A.; Salama S.N.; Salama S.M. (2009). Formulation and characterization of glass – ceramics based on $Na_2Ca_2Si_3O_9$ – $Ca_5(PO_4)_3F$ – Mg_2SiO_4 – system in relation to their biological activity, *Journal Materials Science: Materials in Medicine*, No. 20, pp. 2385 – 2394

Błażewicz S.; Stoch L. (2003). *Biomateriały t4, in: Biocybernetyka i Inżynieria Biomedyczna*, Akademicka Oficyna Wydawnicza, Exit, ISBN 83 – 876474 – 58 – 3, Warszawa, Poland (in Polish)

Brovarone C. ; Verne E. (2006). Macroporous bioactive glasse-ceramic scaffolds for tissue engineering. *Journal of Materials Science: Materials in Medicine,* Vol.17, No.11, pp. 1069-1078

Chen Q.Z.; Efthymiou A. ; SalihV. ; Boccacini A.R. (2008). Bioglass-derived glass-ceramic scaffolds: study of cell proliferation and scaffold degradation in vitro. *Journal of Biomedical Materials Research*, pp. 1049-1060

Czechowska J.; Ślósarczyk A. (2011). Bioaktywne materiały ceramiczne dla inżynierii tkankowej i medycyny regeneracyjnej. *Szkło i Ceramika,* No. 2, pp. 17 – 22 (in polish)

Hee – Gon B.; Sung – Jin K.; Sang – Yeup Park. (2008). Biocompatibility and the physical properties of bio – glass ceramics in the Na2O – CaO – SiO_2 – P_2O_5 system with CaF_2 and MgF_2 additives, *Journal of Ceramic Processing Research*, Vol. 9, No. 6, pp. 588 – 590

Hench L.L. (1998). Biomaterials: a forecast for the future. *Biomaterials*, No.19, pp. 1419 – 1423

Jaegermann Z. (2005). Porowata bioceramika korundowa, praca doktorska, AGH, Kraków, Poland (in polish)

Jaegermann Z. ; Michałowski S. ; Karaś J. ; Chrościcka A. ; Lewandowska – Szumieł M. (2006). Porowate nośniki korundowe do zastosowania w inżynierii tkankowej. *Szkło i Ceramika,* No.57, pp.16 – 20 (in Polish)

Jaegermann Z. ; Ślósarczyk A. (2007). *Gęsta i porowata bioceramika korundowa w zastosowaniach medycznych*, Uczelniane Wydawnictwo Naukowo – Dydaktyczne AGH, Kraków, Poland (in polish)

Krajewski A. ; Ravaglioli A. (2002). Bioceramics and biological glasses. In: *Integrated Biomaterials Science*, Springer US,

Maret D. (2010) et al. Surface expression of precursor N-cadherin promotes tumor cell invasion. *Neoplasia (New York, NY)* 12, pp. 1066-1080

Markul J. (2008). Synergiczne konstrukcje ściernic ze spoiwem ceramicznym, Wydawnictwo Uczelniane Politechniki Koszalinskiej, Monografia, Nr. 156, ISSN 0239 – 7129, Koszalin, Poland (in Polish)

Niżankowski Cz. (2002). Manufacturing sintered corundum abradants. *Archives of Civil and Mechanical Engineering*, No.2, pp. 53 – 64

Puttini S.; Lekka M.; Saugy D.; Dorchies O.; Incitti T.; Bozzoni I.; Kulik A.J.; Mermod N. (2009). Atomic force microscopy assay of the elasticity of utrophin-expressing muscles. *Molecular Therapy*, Molecular Therapy Editorial Office, Seattle

Sachlos E.; Czernuszka J.T. (2003). Making tissue engineering scaffolds work. Review on the application of solid freeform fabrication technology to the production of tissue engineering scaffolds. *European Cells and Materials*, No.5, pp. 29 – 40

Ślósarczyk A. ; Rapacz – Kmita A.(2004). Bioaktywne ceramiczne materiały kompozytowe. *Ceramika Materiały Ogniotrwałe*, Vol.56, No.4, pp. 144 – 149 (in polish)

Staniewicz – Brudnik B.; Lekka M.; Bączek E.; Wodnicka K.; Wilk W. (2010). The effect of the method of obtaining the submicrocrystalline sintered corundum - bioglass composite matrix system on its microstructure and biocompatibility. *Monograph The Faculty of Mechanical Engineering Lodz University of Technology*, pp. 71 – 80, Lodz, Poland

Staniewicz – Brudnik B.; Lekka M.; Jaworska L.; Wilk W. (2010). Biocompatible glass composite system – some physical-mechanical properties of the glass composite matrix system. *Optica Applicata*, Institute of Physics, Wrocław University of Technology, Wrocław, Poland

Szarska S. ; Staniewicz-Brudnik B.; Lekka M. (2008). The effect of the size of the substrate grain made of submicrocrystalline sintered corundum on the bioglass composite structure and certain physico – mechanical properties of the bioglass. *Optica Applicata XXXVIII,* No.1, pp. 251-258

Teramoto H.; et al. (2005). Resorption of apatite – wollastonite containing glass – ceramic and beta – tricalcium phophate in vivo, *Acta Medica Okayama*, Vol. 59, Issue 5

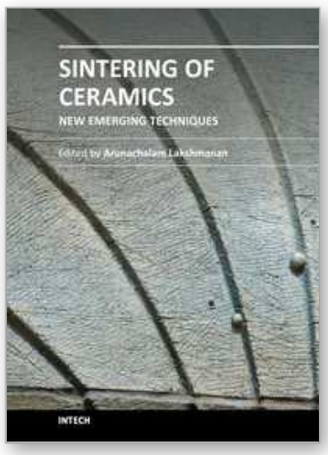

Sintering of Ceramics - New Emerging Techniques
Edited by Dr. Arunachalam Lakshmanan

ISBN 978-953-51-0017-1
Hard cover, 610 pages
Publisher InTech
Published online 02, March, 2012
Published in print edition March, 2012

The chapters covered in this book include emerging new techniques on sintering. Major experts in this field contributed to this book and presented their research. Topics covered in this publication include Spark plasma sintering, Magnetic Pulsed compaction, Low Temperature Co-fired Ceramic technology for the preparation of 3-dimesinal circuits, Microwave sintering of thermistor ceramics, Synthesis of Bio-compatible ceramics, Sintering of Rare Earth Doped Bismuth Titanate Ceramics prepared by Soft Combustion, nanostructured ceramics, alternative solid-state reaction routes yielding densified bulk ceramics and nanopowders, Sintering of intermetallic superconductors such as MgB2, impurity doping in luminescence phosphors synthesized using soft techniques, etc. Other advanced sintering techniques such as radiation thermal sintering for the manufacture of thin film solid oxide fuel cells are also described.

InTech Europe
University Campus STeP Ri
Slavka Krautzeka 83/A
51000 Rijeka, Croatia
Phone: +385 (51) 770 447
Fax: +385 (51) 686 166
www.intechopen.com

InTech China
Unit 405, Office Block, Hotel Equatorial Shanghai
No.65, Yan An Road (West), Shanghai, 200040, China
中国上海市延安西路65号上海国际贵都大饭店办公楼405单元
Phone: +86-21-62489820
Fax: +86-21-62489821

IntechOpen